

THE RELATIONSHIP BETWEEN BLACK HOLE MASS AND VELOCITY DISPERSION IN SEYFERT 1 GALAXIES

CHARLES H. NELSON¹

Physics and Astronomy Department, Drake University, 2507 University Ave.,
Des Moines, IA 50311, charles.nelson@drake.edu

RICHARD F. GREEN^{1,2}

National Optical Astronomy Observatory,
P. O. Box 26732, Tucson, AZ 85726

GARY BOWER¹

Space Telescope Science Institute, 3700 San Martin Drive, Baltimore, MD 21218

KARL GEBHARDT

Department of Astronomy, University of Texas at Austin, Austin, TX 78712

DONNA WEISTROP

Physics Dept., University of Nevada, Las Vegas, Box 4002, 4505 Maryland Pkwy., Las Vegas, NV 89154
Draft version October 8, 2018

ABSTRACT

Black hole masses in active galactic nuclei (AGN) are difficult to measure using conventional dynamical methods, but can be determined using the technique of reverberation mapping. However, it is important to verify that the results of these different methods are equivalent. This can be done indirectly, using scaling relations between the black hole and the host galaxy spheroid. For this purpose, we have obtained new measurements of the bulge stellar velocity dispersion, σ_* , in Seyfert 1 galaxies. These are used in conjunction with the $M_\bullet - \sigma_*$ relation to validate nuclear black hole masses, M_\bullet , in active galaxies determined through reverberation mapping. We find that Seyfert galaxies follow the same $M_\bullet - \sigma_*$ relation as non-active galaxies, indicating that reverberation mapping measurements of M_\bullet are consistent with those obtained using other methods. We also reconsider the relationship between bulge absolute magnitude, M_{bul} , and black hole mass. We find that Seyfert galaxies are offset from non-active galaxies, but that the deviation can be entirely understood as a difference in bulge luminosity, not black hole mass; Seyfert hosts are brighter than normal galaxies for a given value of their velocity dispersion, perhaps as a result of younger stellar populations.

Subject headings: galaxies: nuclei — galaxies: Seyfert — quasars: general — galaxies: kinematics and dynamics

1. INTRODUCTION

An observational problem in research on active galactic nuclei (AGN) is determining the masses of the central black holes. Application of stellar and gas dynamical techniques, commonly used for normal galaxies (e.g. Bower et al. 1998; Gebhardt et al. 2003), is difficult or impossible in type 1 AGN due to the bright nucleus. A potential solution is the technique known as reverberation mapping (Blandford & McKee 1982; Netzer & Peterson 1997), which has been used to estimate black hole masses for about 30 Seyfert galaxies and quasars (Wandel et al. 1999; Kaspi et al. 2000). Rever-

beration mapping allows the radius of the broad line region, R_{BLR} , to be determined by attributing the time lag between variations in the continuum and line emission to light travel time effects. Assuming that the velocity width, W , of the permitted emission lines is due to Keplerian motion in the black hole potential, the mass can be estimated by $M_\bullet \sim W^2 R_{BLR} / G$, where G is the gravitational constant. Thus, this method may provide an opportunity to study the role of the nuclear gravitational potential in large numbers of AGN. But it has not yet been demonstrated that reverberation mapping yields M_\bullet values that are consistent with those obtained from analysis of the stellar and gas dynamics. Given the difficulty of a direct approach, indirect methods must be used to compare these different techniques. Our purpose in this study is to compare reverberation mapping and stellar dynamical measures of black hole mass using scaling relations between the black hole and the host galaxy bulge.

The correlation between black hole mass and

¹ Visiting Astronomer, Kitt Peak National Observatory, National Optical Astronomy Observatory, which is operated by the Association of Universities for Research in Astronomy, Inc. (AURA) under cooperative agreement with the National Science Foundation.

² Kitt Peak National Observatory and National Optical Astronomy Observatory are operated by the Association of Universities for Research in Astronomy, Inc. (AURA) under cooperative agreement with the National Science Foundation.

bulge absolute magnitude, M_{bul} , (Kormendy 1993; Kormendy & Richstone 1995), can be used to compare results of these different approaches. However, comparisons of the M_{\bullet} - M_{bul} relation in active and normal galaxies have produced conflicting results. Two early studies (Ho 1999; Wandel 1999) reported that the reverberation mapping masses for AGN were smaller than the stellar dynamical masses in normal galaxies of the same bulge luminosity. This called into question the validity of the reverberation mapping masses, suggesting a systematic trend to underestimate M_{\bullet} by a factor of ~ 5 (Ho 1999). Alternatively, Wandel (1999) suggested that the masses were accurate and that there were real differences in the black hole masses of active and non-active galaxies of equal bulge mass. More recently, Wandel (2002), revising his early assessment, and McLure & Dunlop (2001), using bulge magnitudes determined in most of their sample from Hubble Space Telescope (HST) images and assuming disk-like kinematics for the BLR, find that active galaxies follow the same $M_{\bullet} - M_{bul}$ relation as normal galaxies.

It is difficult to make a fair assessment of these differing results since some of these studies have used bulge magnitudes derived from the relation between bulge-to-disk ratio as a function of morphological type formulated by Simien & de Vaucouleurs (1986), while others have applied bulge-disk decomposition techniques to ground-based or HST images. Furthermore, bulges of Seyfert galaxies tend to be small — their typical effective radii in all but the nearest objects are a few arcseconds or less. This, combined with the effects of the bright nuclear source in type 1 objects, which are of course the candidates for reverberation mapping, makes ground based estimates of M_{bul} quite tricky.

The relationship between black hole mass and bulge stellar velocity dispersion, σ_* , (Ferrarese & Merritt 2000; Gebhardt et al. 2000a), provides an alternative and independent way to compare stellar dynamical and reverberation mapping results. In this relation, which is stronger than the one using M_{bul} , σ_* is measured in apertures extending to distances of a kiloparsec or so from the nucleus (Gebhardt et al. 2000a, use apertures extending to the bulge effective radius, r_e , and denote their measurement σ_e). The goal is to standardize the region over which the dispersion is determined and more importantly to minimize the influence of the nuclear black hole on the stellar kinematics.

The small number of published σ_* measurements for type 1 AGN, has until recently prevented a statistically significant investigation. Gebhardt et al. (2000b) found no deviation for 7 Seyfert 1s from the $M_{\bullet} - \sigma_e$ relation. The same conclusion was reached by Nelson (2000), using $\text{FWHM}_{[\text{OIII}]}$ in place of σ_* , on the assumption that the forbidden line kinematics in Seyfert galaxies are predominantly the result of virial motion in the bulge gravitational potential (e.g. Nelson & Whittle 1996). Also, Ferrarese et al. (2001) obtained σ_* measurements for 6 Seyfert 1 galaxies and find these values to be consistent with expectations from the $M_{\bullet} - \sigma_*$ relation.

In this paper we present new measurements of σ_* in 14 Seyfert 1 galaxies to check the M_{\bullet} values obtained from reverberation mapping for consistency with the $M_{\bullet} - \sigma_e$ relation established by stellar dynamical techniques. Observations of the Ca II triplet lines and velocity disper-

TABLE 1

Velocity Dispersions in Seyfert 1 Galaxies				
Name	Aperture ($''$)	$\sigma_* \pm \epsilon$ (km/s)	$cz \pm \epsilon$ (km/s)	$\log M_{\bullet}^*$ (M_{\odot})
NGC 3227	4.7	136 \pm 4	1187 \pm 5	7.56 $^{+0.14}_{-0.21}$
NGC 3516	4.3	181 \pm 5	2657 \pm 6	7.23 $^{+0.08}_{-0.09}$
NGC 4051	5.6	89 \pm 3	743 \pm 6	6.15 $^{+0.32}_{-0.45}$
NGC 4151	6.5	97 \pm 3	1020 \pm 6	7.08 $^{+0.23}_{-0.38}$
NGC 4593	6.5	135 \pm 6	2602 \pm 7	6.82 $^{+0.25}_{-0.67}$
NGC 5548	2.2	201 \pm 12	5100 \pm 15	7.97 $^{+0.07}_{-0.07}$
NGC 7469	4.7	131 \pm 5	4947 \pm 7	6.88 $^{+0.30}_{-6.88}$
Mrk 79	4.1	130 \pm 12	6540 \pm 8	8.01 $^{+0.14}_{-0.35}$
Mrk 110	4.7	91 \pm 25	10509 \pm 13	6.89 $^{+0.13}_{-0.21}$
Mrk 279	4.7	197 \pm 12	9062 \pm 12	7.41 $^{+0.10}_{-0.10}$
Mrk 335	—	—	—	6.58 $^{+0.14}_{-0.13}$
Mrk 509	—	—	—	7.96 $^{+0.05}_{-0.06}$
Mrk 590	4.7	189 \pm 6	7904 \pm 7	7.14 $^{+0.10}_{-0.09}$
Mrk 817	4.7	120 \pm 15	9409 \pm 11	7.55 $^{+0.11}_{-0.12}$
Akn 120	3.0	221 \pm 17	9575 \pm 15	8.27 $^{+0.08}_{-0.12}$
3C 390.3	3.6	273 \pm 16	16640 \pm 15	8.57 $^{+0.12}_{-0.21}$

* The black hole masses are those using the r.m.s. BLR widths. Sources are Onken et al. (2003) for NGC 3227, NGC 3516 and NGC 4593, Ho (1999) for NGC 7469 and Kaspi et al. (2000) for the rest.

sion measurements using the Fourier Correlation Quotient (FCQ) are presented in section 2. Bulge magnitude estimates for 11 of these obtained from Hubble Space Telescope archival data are presented in section 3. Notes on individual sample members are presented in section 4. In section 5 we discuss the results in the context of the $M_{\bullet} - \sigma_*$ relation and in section 6 we revisit the $M_{\bullet} - M_{bul}$ relation to try to determine the origin of the discrepancies noted above. Our results are summarized in section 7.

2. SPECTROSCOPIC DATA

2.1. Observations and Reductions

Longslit spectroscopy of 16 Seyfert 1 galaxies and several stellar template stars was obtained on two observing runs (U.T. dates April 10-14, 2001 and November 1-4, 2001) using the 4-meter telescope at Kitt Peak National Observatory. Our sample is composed of Seyfert 1 galaxies included in long term emission line and continuum monitoring campaigns for which reverberation mapping estimates of M_{\bullet} have been published (Kaspi et al. 2000; Wandel et al. 1999; Ho 1999). The RC spectrograph was used with the LB1A CCD which has high quantum efficiency in the far-red ($\sim 90\%$ at 8500 Å), excellent cosmetics and no fringing (Dey et al. 2001) — an ideal detector for observing the Ca II triplet lines ($\lambda 8498.0, \lambda 8542.1$ and $\lambda 8662.1$ Å). These properties allowed us to use a high dispersion grating (BL 380 giving 0.46 Å/pixel in the raw data) and a narrow slit ($1''$) to achieve high spectral resolution ($\sim 1.1\text{Å}$ or $\sim 40 \text{ km s}^{-1}$

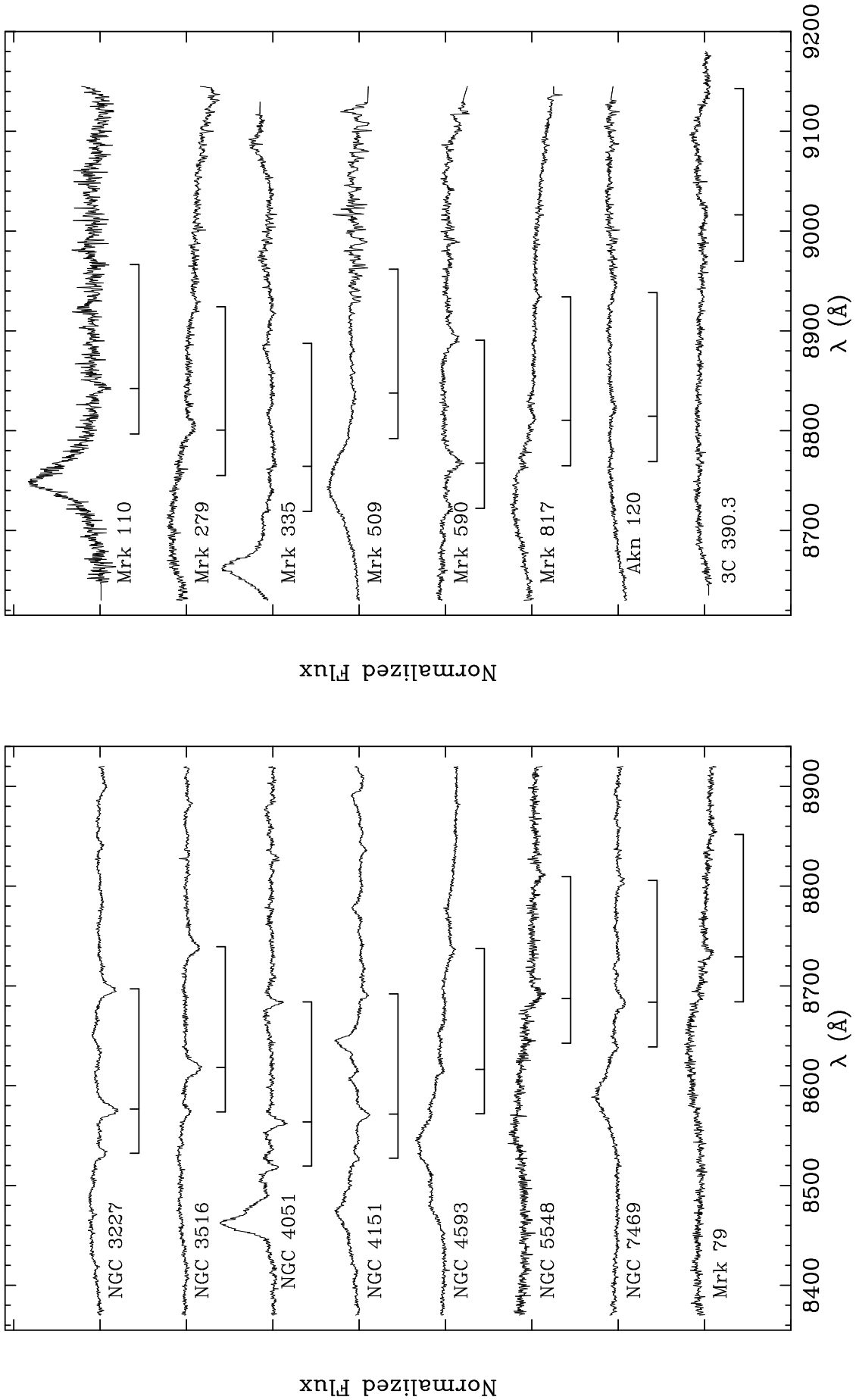


FIG. 1.— Reduced spectra are presented with telluric absorption correction and relative flux calibration applied. The position of the Ca II triplet lines are indicated by the bar with three ticks below each spectrum. The tick marks on the left hand vertical axis indicate the zero points for each spectrum, giving a sense of the broad range in Ca II triplet equivalent width.

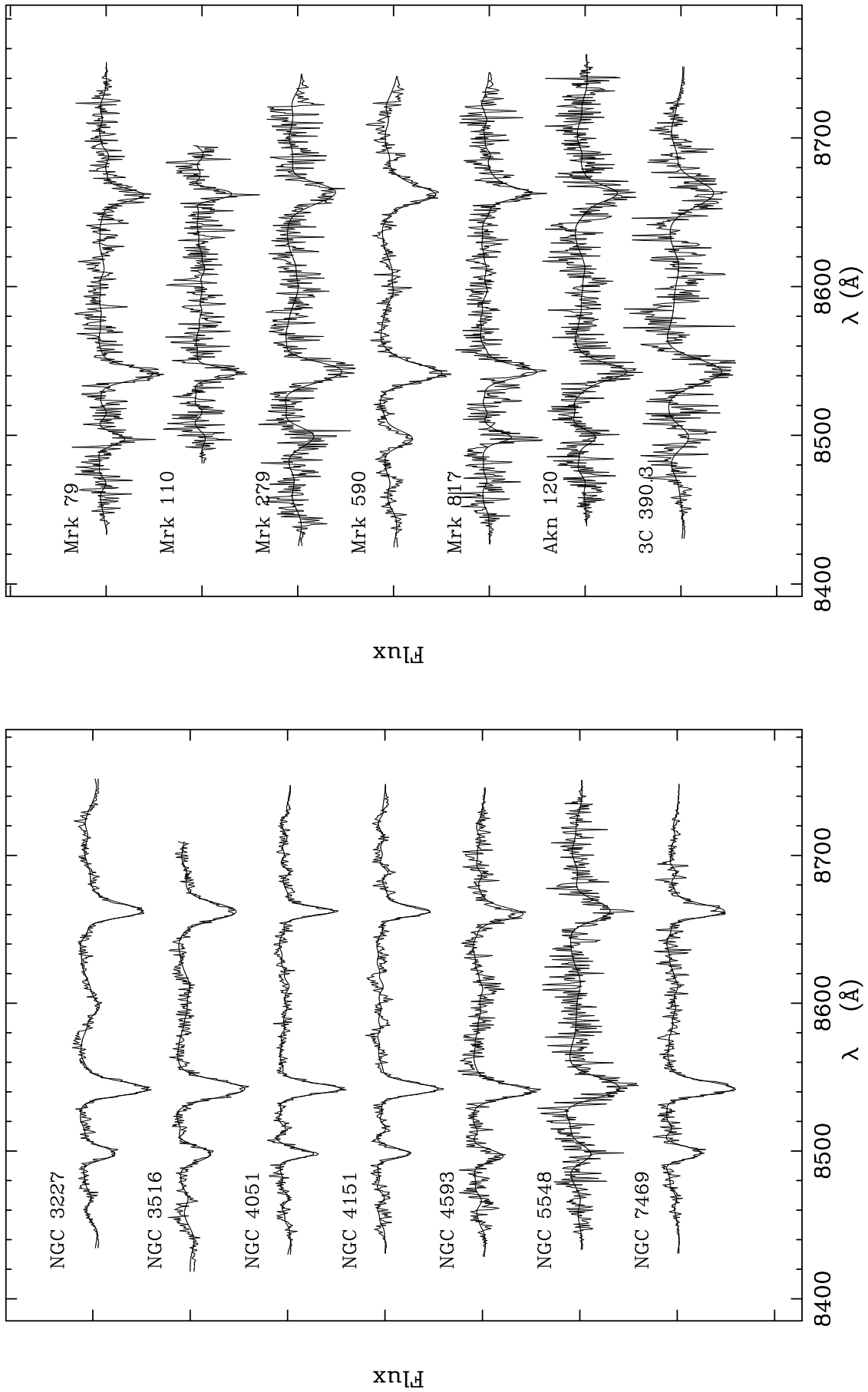


FIG. 2.— We show the finished spectra which were input to FCQ and also the broadened stellar template. The spectra have been scaled so that the middle line in the Ca II triplet has approximately the same depth in each galaxy.

FWHM). We used an order-blocking filter (OG570) to prevent contamination by second-order blue light, which will of course be strong in Seyfert 1 spectra. Exposure times ranged between 3600 seconds for nearby bright galaxies (e.g. NGC 4051, NGC 3516) and 10,800 sec for fainter objects (e.g. Mrk 110). Standard spectroscopic reductions — bias subtraction, flat field correction, geometric distortion and wavelength calibration — were carried out using IRAF. Conditions were generally not photometric so only a relative flux calibration was applied.

The strong telluric emission and absorption features in the far-red present a difficult reduction problem, particularly for the higher redshift galaxies in our sample. For targets with $z \geq 0.016$, where the Ca II triplet and night sky emission lines begin to overlap (except 3C 390.3, see section 4), sky-subtraction was accomplished using the “nod-and-shuffle” observation mode, developed by Glazebrook & Bland-Hawthorn (2001) and recently implemented at Kitt Peak. Briefly, by repeatedly re-positioning the telescope (nodding) and shifting the charge on the detector (shuffling), both the target and the sky are observed at the same spot along the slit and in the same pixels on the detector, permitting excellent sky subtraction. The drawbacks for the nod-and-shuffle technique are a factor of $\sqrt{2}$ increase in the sky noise and extra overhead time for the telescope nods. Although there were difficulties in the implementation of this mode at the time, we were quite pleased with the results and we recommend use of the perfected observing mode where sky subtraction is critical and signal-to-noise is not of primary concern.

Atmospheric absorption bands begin to be a problem at wavelengths above 8900 Å, again affecting the higher redshift members of the sample. Even if the Ca II triplet lines are not directly affected, correction for these can be important for achieving a good fit to the continuum on the red side. We therefore obtained spectra of white dwarf spectroscopic standard stars, matched in airmass and observation time to our Seyfert exposures, to use as atmospheric templates. Experimentation showed that scaling the equivalent width of the atmospheric bands, by adding a constant value to the template and renormalizing, improved the results in some cases, helping to recover good line profiles for the reddest Ca II triplet line. In the case of 3C 390.3, the atmospheric absorption correction was quite critical since all of the Ca II triplet lines lie in a region of strong atmospheric absorption. In part due to the broad Ca II triplet features in this object, we were able to remove the telluric lines successfully.

Reduced, sky-subtracted nuclear spectra corrected for telluric absorption are shown in figure 1. The spectra have been normalized to the mean counts in the spectral region near the Ca II triplet lines, whose positions are indicated for each object. It is worth emphasizing that a variety of spectral characteristics are present in these galaxies. The Ca II triplet lines show a range of equivalent widths presenting a challenge for analysis using the FCQ technique in some cases. Also a number of nuclear emission features, including broad OI $\lambda 8446$, [Fe II] $\lambda 8616$, Paschen and Ca II triplet itself in emission, appear in our spectra and must be removed before analysis with FCQ. In fact for two galax-

ies, Mrk 335 and Mrk 509, no velocity information could be obtained (see section 4). Given the association of AGN and starbursts we must also keep in mind that the strength of the Ca II triplet lines may be enhanced by young stellar populations rich in late-type supergiant stars (e.g. Terlevich, Diaz & Terlevich 1990; Nelson & Whittle 2004).

2.2. Removal of Nuclear Emission

Even in the far-red, the strength of the nuclear emission from type 1 AGN relative to the contribution from the host galaxy makes obtaining high signal-to-noise spectra of the stellar absorption features a difficult task — effectively, the nuclear continuum is a source of noise. Also broad and narrow line nuclear emission, even when not affecting the Ca II triplet lines must be carefully removed before the velocity dispersion measurements can be made. In some cases, where the stellar absorption lines are strong and the nuclear emission is weak, it was possible to include the nucleus of the galaxy in our longslit extractions without further processing. For other galaxies, however, the central rows of the longslit spectra had to be corrected for contaminating emission features, or when the absorption features were entirely lost in the noise, excluded altogether. OI $\lambda 8446$ and [Fe II] $\lambda 8616$ could often be removed by subtraction of a single or double Gaussian fit. In other galaxies the blending of emission lines and continuum was more complex, producing an irregular continuum shape near the Ca II triplet lines. In several cases this required subtraction of a model of the unresolved nuclear spectrum prior to the dispersion measurements.

To produce the model, a narrow spectrum, usually two or three pixels wide centered on the nucleus was extracted. Next, the weak Ca II triplet absorption features were removed from the model by subtracting the spectrum of a stellar template, which was broadened and scaled until the absorption lines vanished. Then, using spectra of nearby ninth or tenth magnitude SAO stars obtained prior to each galaxy exposure, we produced a seeing profile along the slit. This was combined with the model nuclear spectrum and subtracted from the original longslit data to correct for the contamination by the nuclear emission. The most important effect of this procedure is that it removes the irregular continuum shape from spectra immediately adjacent to the nucleus. This was particularly helpful in NGC 4051, NGC 4151 and NGC 4593, where the continuum on the blue side of the spectrum is distinctly uneven (compare figures 1 and 2). This allowed us to extract spectra for the velocity dispersion analysis much closer to the nucleus than would have been possible otherwise, resulting in higher signal-to-noise and ensuring that as much of the bulge light was included as possible.

2.3. Velocity Dispersion Measurements

Velocity dispersions were obtained by analysis of the bulge line-of-sight velocity distribution (LOSVD) using the Fourier-Correlation Quotient method (Bender 1990). For each galaxy a spectral region, including only the Ca II triplet lines and a small section of continuum on either side, was used in the analysis (rest wavelength 8460 Å — 8716 Å). In most cases, the width of the spectrum along the slit was chosen to cover at least 1 kpc

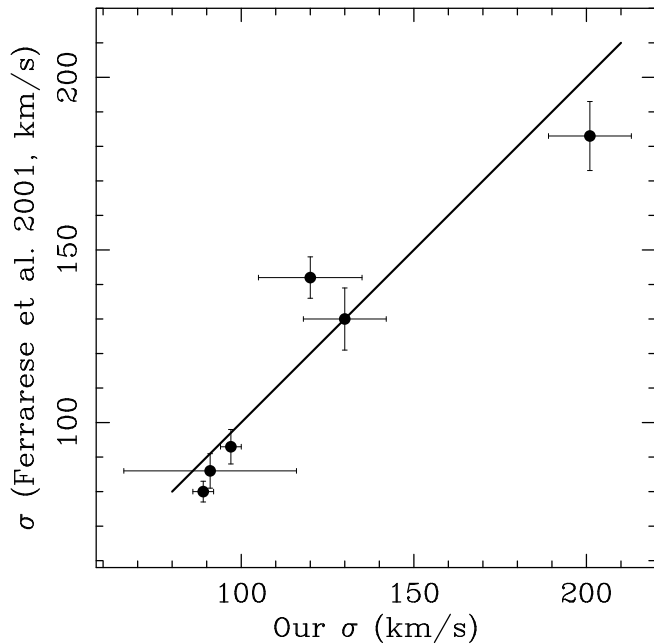


FIG. 3.— Our σ_* measurements are compared with those of Ferrarese et al. (2001). The solid line is $X = Y$.

across each galaxy. For a few nearby galaxies we found that extending the slit all the way out to r_e (see table 2) actually degraded the signal-to-noise while yielding effectively the same dispersion. In these cases we opted for the shorter slit length. For the fainter targets an optimal extraction maximizing signal-to-noise was used. Although this does not generally correspond to r_e as used by Gebhardt et al. (2000a) in defining the $M_\bullet - \sigma_e$ relation, given the difficulties posed by the nuclear emission, it was a reasonable and unavoidable compromise. Nevertheless, our spectra include bulge starlight far enough from the nucleus to be beyond the influence of the black hole, while excluding emission from the kinematically colder galaxy disk.

Gauss-Hermite polynomials were fitted to the LOSVD to determine the bulge systemic velocity, V_* , and the bulge stellar velocity dispersion, σ_* . The uncertainties in V_* and σ_* were estimated by running the FCQ algorithm on Monte Carlo simulations of the data, created using a stellar template convolved with the LOSVD and adding in noise to match that of the observed spectrum. The results for the sample are given in table 1, including M_\bullet values. Figure 2 shows the data used in the FCQ analysis shifted to the rest frame along with the template broadened by the derived LOSVD.

Velocity dispersions for six of our sample galaxies were published by Ferrarese et al. (2001). A comparison of our results with theirs is shown in figure 3. We find that our values agree with theirs quite closely, with a marginal tendency for our dispersions to be larger at the low σ_* end. This may be a consequence of our narrower slit (they used $2''$) which excludes more disk light — a result that may be important for systems with smaller bulges.

3. BULGE MAGNITUDES

To investigate the reported deviations of AGN from the $M_\bullet - M_{bul}$ relation discussed in section 1, we have used archival HST images to measure bulge magnitudes. Ten of the Seyfert 1 galaxies in our sample were observed in the program of WFPC-2 snapshots (Malkan et al. 1998) using the F606W filter and another, NGC 4151, was observed with the F547M filter. The main difficulty in determining the bulge magnitudes from these images was removing the point source nucleus, which is unfortunately saturated in the F606W images. To accomplish this, model PSFs, created using the Tiny Tim software package (Krist 1995), were shifted, scaled and subtracted from the images. The scale factor which produced a minimum r.m.s. deviation in the residual image in an annulus incorporating the innermost unsaturated pixels, was chosen as an initial guess. Since this tends to overestimate the nuclear luminosity, further trial-and-error scaling of the PSF around this value allowed us to fine tune the results; the final best subtraction was judged by examining the removal of peculiar features of the outer PSF (rays and ring like structures) in the residual images. Typically we found that a range of scale factors produced acceptable results. The resulting uncertainty in the bulge magnitudes, which given the subjective nature of the PSF scaling we uniformly take to be $\pm 0^m.2$, was folded into our error estimates. Because the galaxy bulges are reasonably large in the images ($r_e \sim 50 - 100$ pixels in most cases) our results do not depend critically on PSF subtraction. The purpose is mainly to remove the extended wings of the unresolved nuclear emission and recover as much of the inner bulge light as possible. For most objects, we were able to extend our bulge profile analysis down to about half an arcsecond.

Other complications included removing the cosmic ray hits from the images and accounting for emission lines from the Narrow Line Region (NLR). About 90% of the cosmic rays were removed automatically using a script written in IRAF. Of the remaining cosmic rays those close to the nucleus were removed by hand. The broad bandpass of the F606W filter includes the [OIII] $\lambda 5007$, [NII] $\lambda 6548$, $\lambda 6584$, and H α emission lines which arise in the NLR and will not be removed with the point-like nucleus. Using the STSDAS task CALCPHOT, and the model Seyfert 2 galaxy spectrum provided by the SYNPHOT package, we were able to estimate the NLR flux by scaling the model spectrum to match the [OIII] flux tabulated in Whittle (1992a). The [OIII] fluxes are almost all rated quality “a” by Whittle indicating that they were obtained through large apertures and that there is good agreement when more than one measurement has been published. Thus we are confident that we have accounted for the bulk of the NLR emission. This provided a correction to our bulge magnitude estimates and is listed in Table 2.

Ideally, two-dimensional direct fitting techniques, such as that of Peng et al. (2002), and a less restricted model, e.g. a Sersic function, could and should be used to investigate the bulge morphologies of these galaxies. We note in the descriptions of the individual galaxies below (section 4) that the bulge profiles of Mrk 590 and Mrk 817 are better fit by exponentials than $r^{1/4}$ laws. Also some display inner spirals, dust lanes, lenses and bars

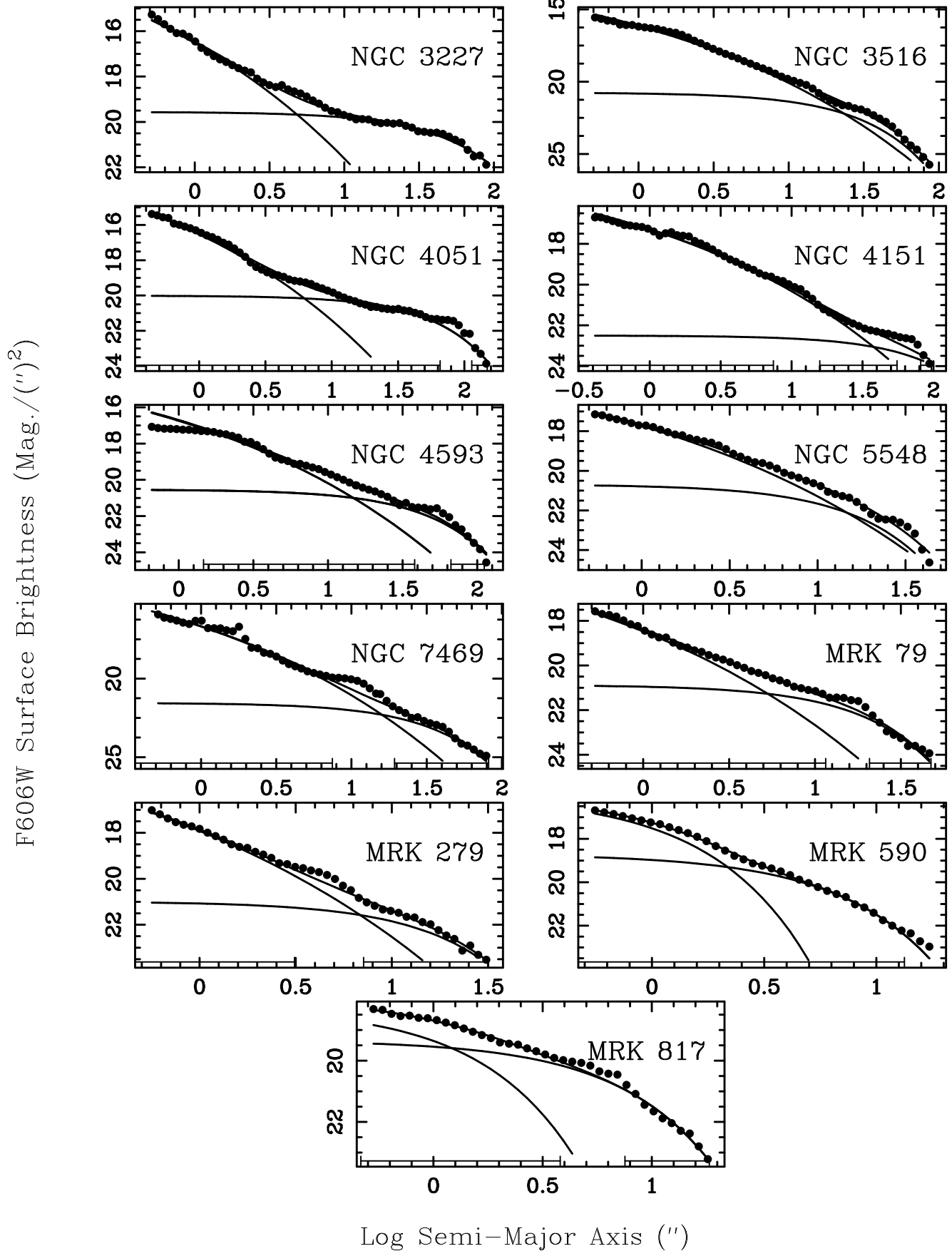


FIG. 4.— Luminosity profiles and bulge-disk decomposition are shown for Seyfert 1 galaxies from HST images. The emission from the nucleus has already been subtracted from the profiles. Note the exponential bulges in Mrk 590 and Mrk 817. A horizontal line shows regions included in the fitting, (if not present all of the data was used) gaps are usually associated with bars.

that further complicate the analysis. However, accounting for these difficulties and the uncertainties associated with NLR emission and saturated PSFs is outside the scope of our program. Thus, in this paper, we adopt either the $r^{1/4}$ law or exponential fits to the azimuthally averaged luminosity profiles and use these to estimate bulge magnitude.

We used the IRAF task ELLIPSE to produce luminosity profiles from the image isophotes which were then fitted with the sum of an exponential or $r^{1/4}$ -law bulge and an exponential disk. In carrying out the fits it is important to avoid getting trapped in spurious minima of χ^2 . The procedure we adopted to ensure meaningful results, was to fit the disk region first. Then holding the disk parameters fixed we included a fit to the bulge. As a final step, we fitted both bulge and disk simultaneously allowing all parameters to vary, using the parameter values from the previous steps as the initial guess. The luminosity profiles and fits are plotted in figure 4. Note the presence of bars or inner ovals in a few galaxies (e.g. NGC 4593, Mrk 79, NGC 7469), seen as a run of excess light over the fit, between the bulge and disk. We generally excluded these regions from the analysis. Bulge magnitudes were then estimated from the scale length and surface brightness parameters of the fits, assuming $H_0 = 75 \text{ km s}^{-1} \text{ Mpc}^{-1}$ (as used by Kaspi et al. 2000, to calculate black hole mass). Foreground extinction from the Milky Way has been removed, but no correction for dust within the host galaxy has been applied. The results are given in table 2 and notes on the characteristics of individual galaxies are given in section 4.

We estimated the error in the bulge magnitudes using Monte Carlo simulations. Random noise with the same r.m.s. deviation as the fit to the luminosity profiles was added to the data and the profile was refitted. The resulting standard deviations in the fit parameters after 30 trials was then propagated through to estimate the error in bulge magnitudes from the fitting. These were then added in quadrature to the uncertainty in the nuclear magnitudes and adopted as the uncertainties listed in table 2. We also include an uncertainty of 15% in the distances of each galaxy to compute the final errors in the absolute magnitudes.

Bulge magnitudes for several of the same Seyfert galaxies were tabulated by McLure & Dunlop (2001), some measured using the same HST images, while others were taken from the photographic study of Baggett, Baggett & Anderson (1998). In figure 5, we plot our values against the McLure & Dunlop (2001) results, where we have corrected their values to our choice of H_0 and to the F606W bandpass (since they quote M_{bul} in the R bandpass). The solid line shows $X = Y$, and suggests no systematic trends, although the large scatter (r.m.s. = 1^m.3, compared with the combined error estimate of 1^m.0) does indicate some disagreement in a number of galaxies. Although McLure & Dunlop (2001) were careful to avoid saturating the nucleus in their own observations of quasar hosts, they do not discuss how they handled the saturated nuclei in the (Malkan et al. 1998) snapshots. Also, in Mrk 817 we have a rather large correction for NLR emission, which to our knowledge was not considered by McLure & Dunlop (2001). In any case the large scatter, while disappointing, is not far outside

TABLE 2

Bulge Magnitudes in Seyfert 1 Galaxies

Name	μ_e^a or μ_0 (mag.) (F606W)	r_e^b or r_0 ($''$)	m_{bul} (mag.) (F606W)	Δm_{NLR} (mag.) (F606W)	M_{bul} (mag.) (F606W)
NGC 3227	18.31 ± 0.16	2.63 ± 0.26	13.24 ± 0.36	0.09	-18.19 ± 0.49
NGC 3516	19.43 ± 0.12	7.41 ± 0.55	11.91 ± 0.29	0.02	-21.19 ± 0.44
NGC 4051	18.58 ± 0.12	3.10 ± 0.23	13.08 ± 0.30	0.05	-18.53 ± 0.44
NGC 4151	21.40 ± 0.09	20.86 ± 1.59	11.52 ± 0.28	0.00	-20.20 ± 0.43
NGC 4593	20.63 ± 0.17	12.44 ± 1.30	12.01 ± 0.37	0.01	-20.87 ± 0.46
NGC 5548	21.49 ± 0.26	11.03 ± 3.20	12.89 ± 0.71	0.06	-21.31 ± 0.78
NGC 7469	19.66 ± 0.14	5.21 ± 0.44	12.93 ± 0.32	0.06	-21.15 ± 0.45
Mrk 79	21.41 ± 0.28	5.68 ± 0.70	14.46 ± 0.45	0.16	-20.29 ± 0.56
Mrk 279	20.31 ± 0.15	3.89 ± 0.41	14.53 ± 0.39	0.06	-20.86 ± 0.51
Mrk 590*	15.99 ± 0.03	0.71 ± 0.02	14.79 ± 0.21	0.03	-20.25 ± 0.39
Mrk 817*	18.25 ± 0.09	0.98 ± 0.13	16.54 ± 0.39	0.44	-18.58 ± 0.51

^a μ_e and μ_0 are the surface brightness fitting parameters for $r^{1/4}$ -law and exponential forms of the luminosity profile respectively.

^b r_e and r_0 are the scale length fitting parameters for $r^{1/4}$ -law and exponential forms of the luminosity profile respectively.

* indicates an exponential bulge was fitted to the data; all others are $r^{1/4}$ law fits.

what might be expected from the uncertainties in the measurements.

4. NOTES ON INDIVIDUAL SEYFERT 1 GALAXIES

NGC 3227 — The active continuum is weak, and the Ca II triplet lines are seen at nearly full strength (Nelson & Whittle 2004). Note the presence of Paschen absorption lines in figure 2 (particularly P14 $\lambda 8598.4$ between the two stronger Ca II triplet lines) indicating the presence of a young stellar population. An F5 III star was used for a velocity template in this case. The bulge of this galaxy is surprisingly small and faint given its Hubble type (SABa de Vaucouleurs et al. 1991) and σ_* , perhaps as a result of the dusty nuclear regions Malkan et al. (1998).

NGC 4051 — Weak Ca II triplet in emission can be seen in this object as well as strong and relatively narrow OI $\lambda 8446$ and [Fe II] $\lambda 8618$ emission. All of these were removed by combining model nuclear emission with a seeing star as described in section 2.2.

NGC 4151 — Nuclear emission features in the Ca II triplet spectrum were removed by combining model nuclear emission with a seeing star. Long and short expo-

sure images for this object were obtained with the F547M filter. This allowed an accurate subtraction of the nucleus. Also this filter excludes most of the optical emission lines so no correction was applied for the NLR. The magnitude in table 2 has been converted to the F606W bandpass using CALCPHOT assuming the spectrum is well represented by the Sb template in the SYNPHOT package. This is the most discrepant point in figure 5, for which McLure & Dunlop (2001) used the bulge-disk decomposition of Baggett, Baggett & Anderson (1998) based on ground based photographic imaging.

NGC 4593 — Nuclear emission features were removed by combining model nuclear emission with a seeing star.

NGC 5548 — Since the velocity dispersion falls off quite rapidly with distance from the nucleus a narrow spectral extraction was used.

NGC 7469 — The position angle and longslit extraction were chosen to avoid knots in the well-known starburst ring (Wilson et al. 1991). OI $\lambda 8446$ was removed with Gaussian fit.

Mrk 110 — This was the poorest spectrum in our sample and as a consequence we quote a large error estimate for the velocity dispersion. OI $\lambda 8446$ removed with Gaussian fit.

Mrk 279 — Broad, weak OI $\lambda 8446$ was removed in normal continuum subtraction.

Mrk 335 — Ca II triplet in emission (Malkan & Filippenko 1983) could not be removed.

Mrk 509 — No Ca II triplet features were detected due to the strong nuclear continuum.

Mrk 590 — The bulge of this galaxy is better fit by an exponential than an $r^{1/4}$ law.

Mrk 817 — OI $\lambda 8446$ was removed with double Gaussian fit. The bulge is better fit by an exponential than an $r^{1/4}$ law.

3C 390.3 — Due to its high redshift, the Ca II triplet lines fall in a region relatively free of night sky emission lines eliminating the need for nod-and-shuffle sky subtraction. However, the atmospheric absorption is severe; careful division by atmospheric template was remarkably successful.

5. THE $M_{\bullet} - \sigma_{*}$ RELATION FOR ACTIVE GALAXIES

In Figure 6 we plot as \bullet symbols our σ_{*} values versus M_{\bullet} values from reverberation mapping. We use the M_{\bullet} values directly from the literature, but note that these are calculated assuming random orbits for BLR clouds following equation 5 in Kaspi et al. (2000) (see also Wandel et al. 1999). We discuss the significance of this assumption in section 6. Furthermore, as mentioned in the note to table 1, the black hole masses are those calculated using the r.m.s. $H\beta$ FWHM rather than the mean values, i.e. the variable component of the line (see Wandel et al. 1999). Having tried both, we find no significant differences in our results using one or the other. For comparison, we also plot as $+$ symbols, elliptical and S0 galaxies from Gebhardt et al. (2000a), where M_{\bullet} has been determined from stellar dynamical orbit-based modeling. The solid line is the derivation of the $M_{\bullet} - \sigma_{e}$ relation from Tremaine et al. (2002) and the dashed line is a fit to the Seyferts using the ordinary least squares bisector method (hereafter OLSB, Isobe et al. 1990). The fourteen Seyferts, by themselves, show a strong correlation (linear correlation coefficient, $R = 0.73$ for the r.m.s.

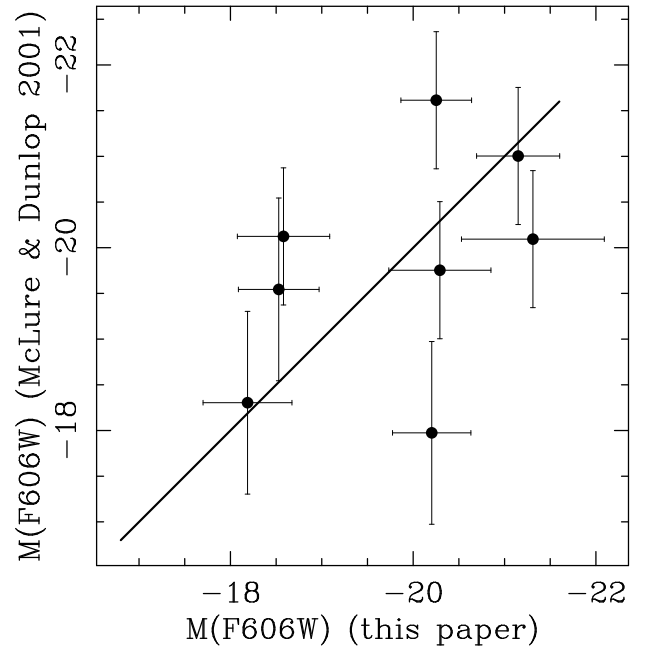


FIG. 5.— Our M_{bul} measurements are compared with those of McLure & Dunlop (2001) rescaled to rescaled to $H_0 = 75 \text{ km s}^{-1} \text{ Mpc}^{-1}$. The solid line is $X = Y$.

masses with probability of no correlation, $P_{null} = 0.29\%$ and slightly better for the mean masses $R = 0.80$, and $P_{null} = 0.065\%$).

In figure 6 there appears to be no significant evidence for an offset for Seyferts from the Tremaine et al. (2002) relation. Computing the residuals of the AGN to the solid line we find an average shift of $\Delta \log M_{\bullet} = 0.21$ in the direction of lower black hole masses at a given σ_{*} , with a standard deviation of 0.46 dex for the 14 AGN. Clearly, the significance of such a shift is marginal and distinctly not in agreement with the factor of 5 found by Ho (1999) using the $M_{\bullet} - M_{bul}$ relation.

The exact value of the slope of $M_{\bullet} - \sigma_{*}$ has been a matter of some debate. The slope, 4.1 ± 0.5 for the AGN sample is not significantly different from the slope for the normal galaxies, although given the uncertainty, it is beyond the ability of this dataset to provide a decisive result. A larger sample of AGN might well provide interesting constraints.

These results effectively confirm the conclusions of Gebhardt et al. (2000b), Nelson (2000) and Ferrarese et al. (2001) that there is no distinct difference in the $M_{\bullet} - \sigma_{e}$ relation between active and non-active galaxies. Furthermore, it suggests that the reverberation mapping technique for determining black hole masses in AGN produces results which are consistent with masses determined by stellar and gas dynamical techniques. We should emphasize, however, that this is an indirect check on reverberation mapping. A direct verification may be possible should a target of reverberation mapping campaigns go into a low luminosity phase, allowing application of standard stellar dynamical analysis. Indeed an HST cycle 12 proposal involving target of opportunity observations of NGC 3227 and NGC 4151 has been approved (Prop. No. 9849, PI B. Peterson).

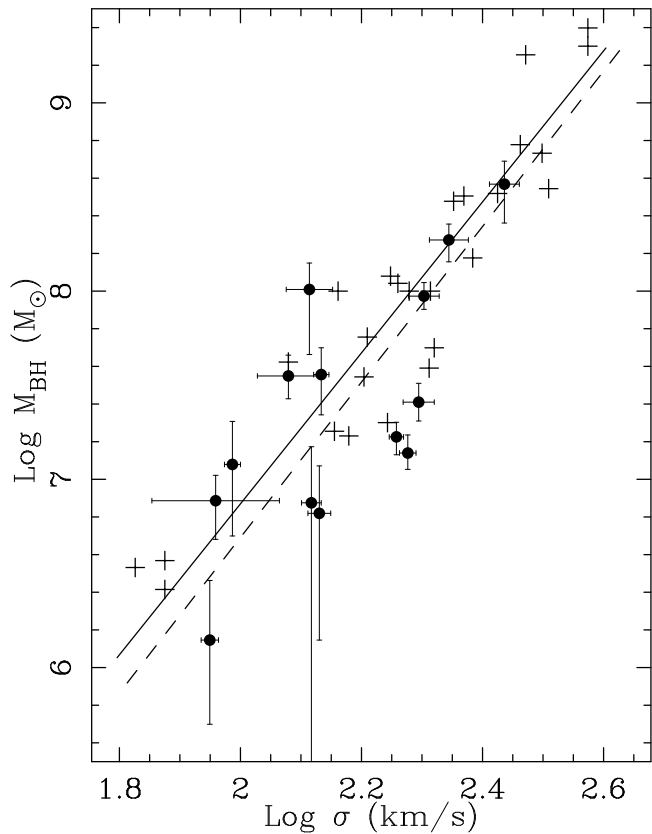


FIG. 6.— Black hole mass is plotted against velocity dispersion for Seyfert galaxies from Table 1, shown as \bullet symbols and for normal elliptical and S0 galaxies from Gebhardt et al. (2000a), shown as $+$ symbols. The black hole masses for Seyfert galaxies are determined from reverberation mapping, while the Gebhardt et al. (2000a) masses are from dynamical modeling of the nuclear stellar kinematics. The solid line is the relation calculated by Tremaine et al. (2002) and the dashed line is a fit to the Seyferts using the ordinary least-squares bisector method (Isobe et al. 1990).

Our results, of course, are very encouraging for investigations of the role of black hole mass in AGN. However, the sample used here is by necessity composed of lower luminosity Seyfert 1 galaxies. Further study of the $M_{\bullet} - \sigma_e$ relation is needed to validate its application to more luminous AGN.

6. THE $M_{\bullet} - M_{bul}$ RELATION FOR AGN REVISITED AND THE FABER-JACKSON RELATION

It is essentially conventional wisdom that active nuclei are preferentially found in bulge dominated galaxies (e.g. Ho, Filippenko & Sargent 1997). Confirmation of the $M_{\bullet} - \sigma_*$ relation for Seyferts is important support for this tenet of AGN physics. It strongly reinforces the notion that the bulge gravitational potential plays an important role in determining the properties of activity in galaxies. However, if we accept that the $M_{\bullet} - \sigma_*$ relation is the same for Seyferts as it is for normal bulges and ellipticals, what do we make of previous claims of smaller M_{\bullet} values in AGN for a given bulge luminosity, discussed in the introduction to this paper?

In Figure 7 we plot M_{bul} for the Seyfert 1 galaxies in table 2, versus the reverberation mapping M_{\bullet} values. Again for comparison, ellipticals and bulges from the Gebhardt et al. (2000a) sample, are plotted as $+$ sym-

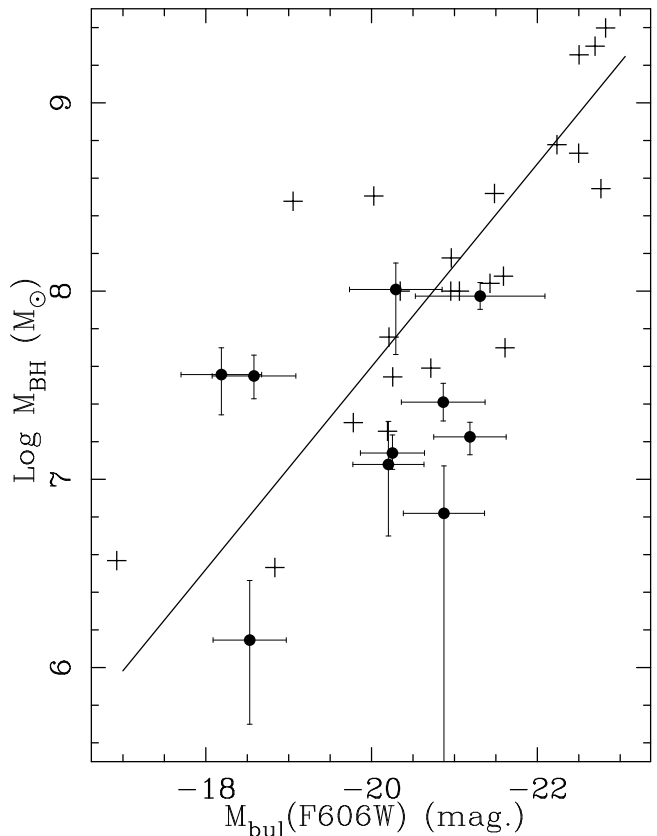


FIG. 7.— Black hole mass is plotted against bulge absolute magnitude for Seyfert galaxies (\bullet symbols) and the Gebhardt et al. (2000a) sample ($+$ symbols) rescaled to $H_0 = 75 \text{ km s}^{-1} \text{ Mpc}^{-1}$. The solid line is a fit to the elliptical galaxies.

bols, where we have converted their absolute V magnitudes as published in Faber et al. (1997) to the F606W bandpass and scaled to $H_0 = 75 \text{ km s}^{-1} \text{ Mpc}^{-1}$. Given the narrow range of colors for the Gebhardt et al. (2000a) sample ($\langle B - V \rangle = 0^m95$, std. dev. 0^m047) and the expectation that the Seyfert bulge colors are likely to be more scattered, we choose to apply the correction to the ellipticals. The conversion was determined using the template elliptical galaxy from the SYNPHOT package and the CALCPHOT task ($M_{F606W} = V - 0^m33$).

Although not a strong trend, the majority of Seyferts lie below and to the right of the OLSB fit to the ellipticals, shown as the solid line. This is consistent with the report by Ho (1999) of lower black hole masses at a given bulge magnitude. The median deviation in black hole mass for the Seyferts from the fit to the normal galaxies is 0.4 dex, or about a factor of 2.5. There is really no significant correlation for the Seyferts, (linear correlation coefficient $R = -0.16$), compared with a strong trend found for the ellipticals ($R = -0.80$). This may be due in part to the smaller sample size, but this cannot be the whole story since the Seyferts show a strong correlation between M_{\bullet} and σ_* (see section 5).

We suggest that it is the bulge luminosities, not the black hole masses, which are the origin of the deviation. Taken in this way the bulges of Seyferts are on average 0^m7 brighter than normal ellipticals with similar black hole masses based on the distribution of points in figure 7. Strong support for this interpretation is found by

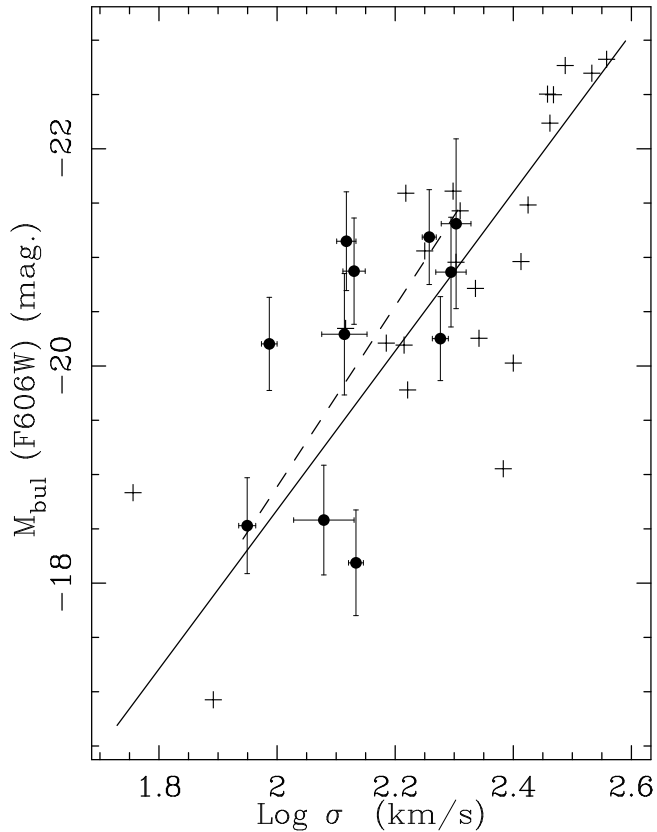


FIG. 8.— The Faber-Jackson plot for Seyfert 1 galaxies from Table 2 (● symbols) and for elliptical and S0 galaxies from Gebhardt et al. (2000a, + symbols). The solid line is a fit to the elliptical sample and the dashed line is a fit to the Seyfert galaxies. The Seyfert galaxies in the sample show a tendency for brighter M_{bul} at a given σ_* .

plotting the Faber-Jackson diagram, σ_* vs. M_{bul} , for both samples, shown in fig. 8. We find that at a given σ_* the Seyfert galaxies tend to lie above the fit to the normal galaxies. The mean residual in M_{bul} for the Seyferts relative to the normal galaxy fit is $-0^m.4$. Furthermore there is a moderately strong correlation for the Seyferts, ($R = -0.6$). This improvement over the results for M_{bul} vs. M_\bullet naturally suggests that M_{bul} is more closely related to σ_* than to M_\bullet , and that the increase in bulge luminosities with black hole masses is secondary and follows through their mutual trends with velocity dispersion.

The result is identical to that of Nelson & Whittle (1996) who found a similar offset for a much larger sample, consisting of mostly Seyfert 2s. The result also confirms the earlier conclusions of Whittle (1992b,c) who used galaxy rotation amplitude and $FWHM_{[OIII]}$ as virial parameters, to demonstrate a tendency for brighter bulges in Seyferts than normal galaxies of the same bulge mass. Some ambiguity remained, however, since the bulge magnitudes in those studies were not obtained by bulge/disk decomposition. Instead, after correcting for nuclear emission, the relation between bulge-to-disk ratio and Hubble stage of Simien & de Vaucouleurs (1986) was used to estimate bulge magnitudes. This technique has been criticized by McLure & Dunlop (2001) and Wandel (2002) who suggest that it results in overestimates of

M_{bul} . The present confirmation of the offset in the Faber-Jackson relation for Seyferts using explicit bulge-disk-nucleus separation, however, suggests that while there is admittedly significant scatter, any systematic errors are small.

In contrast to the Ho (1999) result, McLure & Dunlop (2001) and Wandel (2002) claim no deviation in the $M_\bullet - M_{bul}$ relation for Seyfert and normal galaxies. We can reconcile this conflict by recognizing that McLure & Dunlop (2001) choose to calculate M_\bullet assuming a disk-like morphology and purely rotational kinematics for the BLR as opposed to random orbits assumed by Kaspi et al. (2000). Thus the observed line widths depend on the orbital velocity, V , and the inclination of the BLR disk. After making assumptions about the range and mean of the distribution of inclinations, they adopt a relation between orbital velocity and the BLR line widths, $V = 1.5 \times FWHM$, distinctly different from the case for random cloud orbits, $V = \sqrt{3}/2 \times FWHM$. This results in M_\bullet values that are a factor of 3 larger than the standard reverberation mapping calculations in which the BLR velocity field is assumed to be random. Therefore, if we were to couple their bulge measurements with the M_\bullet values calculated assuming random BLR motions, we should also get brighter bulges at a given M_\bullet for AGN. Of course the specific form of the BLR velocity field is unknown. Our results, at least for the case of random cloud motions, are consistent with an identical $M_\bullet - \sigma_e$ relation for Seyfert and normal galaxies, and a tendency for brighter bulges in Seyferts.

A different argument applies to the Wandel (2002) analysis, which assumes random motions dominate in the BLR. This study reports a correlation between $H\beta$ line width and the suspected overestimate of M_{bul} resulting from the application of the Simien & de Vaucouleurs (1986) B/T -morphology relation discussed above. This correlation is then used to correct the M_{bul} values, resulting in a reduction of the bulge luminosities for much of the sample. However, the physical link between BLR kinematics and differences in B/T is not established. It is therefore unclear why such a correction should be required. Removing this correction from Wandel's results should also result in relatively brighter bulges for AGN.

The most straightforward interpretation of these results is that Seyfert galaxies have, on average, brighter bulges as a result of lower M/L ratios. Thus, the difference is one of stellar population, indicating that Seyferts are more likely than non-active galaxies to have had recent episodes of nuclear star formation. This is certainly plausible, given the voluminous research on the link between AGN and starburst galaxies. It is informative to use model stellar populations to estimate the age and mass fraction of the bulge required to produce a brightening of this degree. Guy Worthey's Dial-a-Galaxy website (Worthey 1994) allows users to mix stellar population models of different ages, metallicities, etc., to estimate the changes to the integrated light properties of galaxy spectra. A simple run, with two solar metallicity populations of 1 Gyr and 12 Gyr, shows that if 15% of the total mass is from the young population the R -band magnitude will be $\sim 0^m.5$ brighter than a population composed of completely old stars. Obviously more complex and realistic models could produce similar results. Neverthe-

less, this simple estimate indicates a typical size and age for a burst of star formation to produce the shift seen in the Seyfert sample.

It is interesting to note that a number of recent morphological studies of Seyfert galaxies have found no evidence for morphological triggers of nuclear starbursts — galaxy interactions and bars, including sub-kpc scale bars (e.g. Ho, Filippenko & Sargent 1997; Pogge & Martini 2002; Regan & Mulchaey 2001). Although it is conceivable that there is a time delay between a galaxy interaction and the onset of nuclear fueling, the result is troubling since we might expect at least some evidence of the disturbance to remain. A possible solution was hinted at in Nelson & Whittle (1996) based on the fact that Seyferts are not found outside the general envelope of scatter for normal galaxies in the Faber-Jackson plot. Considering the residuals to the Faber-Jackson relation, they found that the distribution of $\Delta \log \sigma_*$ is considerably narrower yet overlapping that for non-active galaxies, a detail which is reproduced in Figure 8. Assuming that the spheroids of normal galaxies exhibit a broad range of star-formation histories, perhaps Seyferts are more akin to normal spirals with above average central star formation rates than to massive starbursts initiated by strong interactions or bars.

7. SUMMARY

We have obtained new measurements of the bulge stellar velocity dispersion in Seyfert 1 galaxies with nuclear black hole masses determined using the reverberation mapping technique. Our results have shown that Seyfert galaxies follow the same correlation between M_\bullet and σ_* as for non-active galaxies and that reverberation mapping yields black hole masses which are consistent with masses determined through stellar dynamical modeling techniques. We also investigated the origin of previous assertions that the masses of black holes in active galaxies were smaller than those in normal galaxies (or at least underestimated) at a given bulge luminosity. We find that the best explanation is that the bulges are brighter on average in Seyfert galaxies, suggesting lower M/L ratios, most likely as a result of higher star formation rates in their recent history.

We would like to thank the Kitt Peak staff for their help with the observations using the new LB1A chip. In particular we would like to thank Arjun Dey for his help with the “nod-and-shuffle” sky subtraction which proved critical in our analysis.

REFERENCES

- Baggett, W. E., Baggett, S. M. & Anderson, K. S. J. 1998, *AJ*, 116, 1626
- Bender, R. 1990, *A&A* 229 441
- Blandford, R. D., & McKee, C. F. 1982, *ApJ*, 255, 419.
- Bower, G. A., et al. Green, R. F., Danks, A., Gull, T., Heap, S., Hutchings, J., Joseph, C., Kaiser, M. E., Kimble, R., Kraemer, S., Weistrop, D., Woodgate, B., Lindler, D., Hill, R. S., Malumuth, E. M., Baum, S., Sarajedini, V., Heckman, T. M., Wilson, A. S. & Richstone, D. O. 1998, *ApJ*, 492, L111
- de Vaucouleurs, G., de Vaucouleurs, A., Corwin, H. G., Jr., Buta, R. J., Paturel, G. & Fouqué, P. 1991, *The Third Reference Catalogue of Bright Galaxies* (New York: Springer)(RC3).
- Dey, A. et al. March 2001, *NOAO Newsletter* No. 65 p. 37
- Faber, S. M., Tremaine, S. Ajhar, E. A. Byun, Y., Dressler, A., Gebhardt, K., Grillmair, C., Kormendy, J., Lauer, T. R. and Richstone, D. 1997, *AJ*, 114, 1771
- Ferrarese, L. & Merritt, D. 2000, *ApJ*, 539, L9
- Ferrarese, L. Pogge, R. W., Peterson, B. M., Merritt, D., Wandel, A., & Joseph, C. L. 2000, *ApJ*, submitted
- Gebhardt, K., et al. Bender, R., Bower, G., Dressler, A., Faber, S. M., Filippenko, A. V., Green, R., Grillmair, R., Ho, L. C., Kormendy, J., Lauer, T. R., Magorrian, J., Pinkney, J., Richstone, D., Tremaine, S. 2000, *ApJ*, 539, 13
- Gebhardt, K., Richstone, D., Tremaine, S., Lauer, T. R., Bender, R., Bower, G., Dressler, A., Faber, S. M., Filippenko, A. V.; Green, R., Grillmair, C., Ho, L. C., Kormendy, J., Magorrian, J., Pinkney, J. 2003 *ApJ*, 583, 92
- Gebhardt, K., Kormendy, J., Ho, L. C., Bender, R., Bower, G., Dressler, A., Faber, S. M., Filippenko, A. V., Green, R., Grillmair, R., Lauer, T. R., Magorrian, J. Pinkney, J., Richstone, D. Tremaine, S. 2000, *ApJ*, 543, L5
- Glazebrook, K. & Bland-Hawthorn, J. 2001, *PASP*, 113, 197
- Ho, L. C. 1999, in *Observational Evidence for Black Holes in the Universe*, ed. S. K. Chakrabarti (Dordrecht:Kluwer), 153
- Ho, L., Filippenko, A. V. & Sargent, W. L. W. 1997, *ApJ*, 487, 568
- Isobe, T., Feigelson, E. D., Akritas, M., G., & Babu, G. J., 1990, *ApJ*, 364, 104
- Kaspi, S., Smith, P. S., Netzer, H., Maoz, D., Januzzi, B. T., & Giveon, U. 2000, *ApJ*, 533, 631
- Kormendy, J. 1993, in *The Nearest Active Galaxies*, ed. J. Beckman, L. Colina, & H. Netzer (Madrid: Consejo Superior de Investigaciones Científicas), 197
- Kormendy, J. & Richstone, D. 1995, *ARA&A*, 33, 581
- Krist, J. 1995, in *ASP Conference Series*, Vol. 77, *Astronomical Data Analysis Software and Systems IV*, eds. R.A. Shaw, H.E. Payne, and J.J.E. Hayes (San Francisco: ASP) p. 349
- Laor, A. 2000, *ApJ*, in press.
- Malkan, M. A., & Filippenko, A. V. 1983, *ApJ*, 275, 477.
- Malkan, M. A., Gorjian, V., Tam, R. 1998, *ApJS*, 117, 25
- Magorrian, J., Tremaine, S., Richstone, D. Bender, R. Bower, G., Dressler, A. Faber, S. M.; Gebhardt, K. Green, R. Grillmair, C., Kormendy, J., & Lauer, T. 1998, *AJ*, 115, 2285
- McLeod, K. K., & Reike, G. 1994, *ApJ* 431, 137
- Mclure, R. J. & Dunlop, J. S. 2001, *MNRAS*, 321, 199
- Nelson, C. H. 2000, *ApJ*, 544, L91
- Nelson, C. & Whittle, M. 1995, *ApJS*, 99, 67
- Nelson, C. & Whittle, M. 1996, *ApJ*, 465, 96
- Nelson, C. & Whittle, M. 2004, in preparation.
- Netzer, H., & Peterson, B. M. 1997, in *Astronomical Time Series*, ed. D. Maoz, A. Sternberg, & E. M. Leibowitz (Dordrecht: Kluwer), 85
- Onken, C. A., Peterson, B. M., Dietrich, M., Robinson, A., Salamanca, I. M. 2003 *ApJ*, 585, 121
- Peng, C., Ho, L. C., Impey, C. D., Rix, H. 2002, *AJ*, 124, 266
- Peterson, B. & Wandel, A. 1999, *ApJ*, 521, 95
- Pogge, R. & Martini, P. 2002, *ApJ* 569, 624
- Regan, M. & Mulchaey, J. 1999 *AJ*, 117, 2676
- Simien, F., & de Vaucouleurs 1986, *ApJ*, 302, 564
- Smith, E. P., Heckman, T. M. & Illingworth, G. D. 1990, *ApJ*, 356, 399
- Terlevich, E., Diaz, A. I. & Terlevich, R. 1990, *MNRAS*, 242, 271
- Tremaine, S. 2002, *ApJ*, 574, 740
- Wandel, A., Peterson, B. M., & Malkan, M. A. 1999, *ApJ*, 526, 579
- Wandel, A. 1999, *ApJ*, 519, L39
- Wandel, A. 2002, *ApJ*, 565, 762
- Whittle, M. 1992 a, *ApJS*, 79, 49
- Whittle, M. 1992 b, *ApJ*, 387, 109
- Whittle, M. 1992 c, *ApJ*, 387, 121
- Wilson, A. S., Helfer, T. T., Haniff, C. A. & Ward, M. J. 1991, *ApJ*, 381, 79
- Worthey, G. 1994, *ApJS*, 95, 107